SPRAY COMBUSTION AT NORMAL AND REDUCED GRAVITY IN COUNTERFLOW AND CO-FLOW CONFIGURATIONS

Alessandro Gomez and Gung Chen
Department of Mechanical Engineering
Yale University, P.O. Box 208286, New Haven, CT 06520-8286

Introduction

Liquid fuel dispersion in practical systems is typically achieved by spraying the fuel into a polydisperse distribution of droplets evaporating and burning in a turbulent gaseous environment. In view of the nearly insurmountable difficulties of this two-phase flow, a systematic study of spray evaporation and burning in configurations of gradually increasing levels of complexity, starting from laminar sprays to fully turbulent ones, would be useful. A few years ago we proposed to use an electrostatic spray of charged droplets for this type of combustion experiments under well-defined conditions. In the simplest configuration, a liquid is fed into a small metal tube maintained at several kilovolts relative to a ground electrode few centimeters away. Under the action of the electric field, the liquid meniscus at the outlet of the capillary takes a conical shape, with a thin jet emerging from the cone tip (cone-jet mode). This jet breaks up farther downstream into a spray of charged droplets — the so-called ElectroSpray (ES). Several advantages distinguish the electrospray from alternative atomization techniques: 1) it can produce quasi-monodisperse droplets over a phenomenal size range; ii) the atomization, that is strictly electrostatic, is decoupled from gas flow processes, which provides some flexibility in the selection and control of the experimental conditions; iii) the Coulombic repulsion of homopolarly charged droplets induces spray self-dispersion and prevents droplet coalescence; iv) the ES provides the opportunity of studying regimes of slip between droplets and host gas without compromising the control of the spray properties; v) the compactness and potential controllability of this spray generation system makes it appealing for studies in reduced-gravity environments aimed at isolating the spray behavior from natural convection complications. With these premises, in March 1991 we initiated a series of experiments under NASA sponsorship (NAG3-1259 and 1688) in which the ES was used as a research tool to examine spray combustion in counter-flow and co-flow spray diffusion flames, as summarized below. The ultimate objective of this investigation is to examine the formation and burning of sprays of liquid fuels, at both normal and reduced gravity, first in laminar regimes and then in turbulent ones.

Summary of the Research Activity from 9-1-92 to 3-15-95

The investigation focused initially on cold flow experiments aimed at examining the fundamental mechanism of electrospray atomization and dispersion, as well as at identifying and characterizing the domain of operating variables under which monodisperse droplets were generated. Once we could synthesize sprays of desired properties, as documented in refs. 1-5, we focused on the combustion of such electrosprays in laminar counterflow and co-flow spray burners at both normal and reduced gravity. The primary diagnostic tool at normal gravity was a commercial Phase Doppler Anemometer (PDA) used to measure distributions of droplet size and either axial or radial velocity component. Heptane, doped with 0.3% (by weight) of an antistatic additive to increase its electric conductivity, was used in all the experiments.

Laminar Counterflow Diffusion Flames—Normal Gravity

Spray combustion was first examined in a counterflow configuration comprising two opposed jets, with oxygen fed from one side and an heptane electrospray in a co-flow of nitrogen fed from the other side. Initially we studied the combined effects of changes in droplet size, velocity and strain rate, as discussed in ref. 6 and at the last Microgravity Workshop (ref. 7). More recently, we examined the individual effect of each variable in similar flames in which CO_2, for reasons to be discussed below, was used as diluent (ref. 8). Initial droplet size and velocity were found to affect significantly the flame appearance, its thermal structure and pollutant formation, whereas the strain rate and its effect on the inertia behavior of the droplets plays a role less important than the other two controlling variables. When droplets evaporate completely before reaching the flame, a blue spray flame is stabilized that in many respects is like an ordinary gaseous flame in which the droplets simply act as a source of vapor that is convected and diffuses towards the flame. Alternatively, if insufficient time is available for the droplets to evaporate in their journey towards the flame, they penetrate it and continue to burn on the oxidizer side, leading to a complex and thick flame zone, that is also characterized by soot formation. In the latter case, there is also some evidence of individual droplet burning. Droplet/flame interaction can be usefully interpreted in terms of a Damkhöler number of evaporation, that is the ratio of a droplet residence time and the droplet evaporation time. Namely

$$Da_{ev} = \frac{t_r}{t_{ev}} = \frac{z_i \overline{K}}{V_D D^2}$$

where D is the droplet diameter, $\bar{K}$ is an average evaporation coefficient; z_f is the location of the blue flame formed by the fuel vapor and the oxidizer, and $\bar{V}_D$ is the average droplet velocity. When $Da_{ev} \geq 1$, droplet evaporation is completed on the fuel side of the vapor flame. Whereas, when $Da_{ev} < 1$, the complex flame structure ensues, with droplets overshooting the vapor diffusion flame. Such conditions are achievable with large droplets, large initial velocities or relatively unvolatile liquids.

An interesting byproduct of the combustion of electrostatic sprays is the occurrence of a secondary atomization when, in the course of the droplet evaporation, the electric charge density on the droplet surface increases until the so-called Rayleigh limit is reached. At this point, the repulsion of electric charges overcomes the surface tension cohesive force, ultimately leading to a disintegration into finer fragments. We completed an investigation on this phenomenon (ref. 9), that had been previously demonstrated in non-reactive environments (ref. 2). Charge-induced secondary atomization may be inhibited if direct droplet-flame interaction occurs, in which case the concentration of flame chemi-ions or electrons is sufficient for them to neutralize the charge on the droplets and thus prevent disruption. This result can be rationalized in terms of a non-dimensional number involving the Debye length, that is a characteristic length over which charge separation is induced locally by the thermal motion of charge carriers of disparate molecular mass in an electrically neutral flame. This length is on the order of a few microns in a typical flame. Only if the droplets are within such a short distance from the flame, as is the case when they actually penetrate it, neutralization does occur. Since the bulk of a "well-behaved" spray should burn with the dispersed phase all on the fuel side, i.e. without droplets overshooting the flame, charge-induced secondary atomization will occur, provided, of course, that the droplets have been charged at the injection. This approach could be practically implemented in electrostatically-assisted atomizers. We estimated that total mass loss due to multiple disruptions is approximately 7% of the droplet mass at the time of the first disruption. Since, in consideration of their size, the offspring vaporize instantaneously on the time scale of the parent droplet life, the mass loss upon disruption is "immediately" available as vapor. Thus, the disruption process would enhance the evaporation rate of a non-negligible fraction of the liquid supply and also aid in the overall stabilization of the spray flame.

Laminar Counterflow Diffusion Flames—Experiments in the 2.2s Drop Tower at NASA Lewis
We retrofitted the counter-flow spray diffusion flame burner for experiments in the 2.2 s drop-tower at NASA-Lewis that took place in April, 1993. These tests demonstrated that the electrospray is a compact spray injector system that is well-suited for the confinements of typical low gravity environments. We recorded on videotape microgravity-induced changes in the appearance of the same spray flames that had been examined at normal gravity. What used to be flat flames at normal gravity appeared now as capped, mushroom-shaped ones. The microgravity tests clearly showed that the flame flatness was apparently a buoyancy artifact and that "edge" effects were actually affecting the entire flame. Notice that the two-dimensionality of the flame would be a major drawback, especially from a computational vantage point. The observed effect was tentatively attributed to the velocity profiles at the burner mouth. On the fuel side, in fact, the need to minimize the interception of the droplets on their way to the flame imposed the use of a screen made of very thin wire that evidently did not adequately uniformize the axial velocity profile, in which case a transitional regime between a plug flow and a fully-developed Hagen-Poiseuille profile would be established. Stoichiometric requirements and constraints on the electrospray flow rates prevented us from modifying the velocity profile by changes in feed rates. Thus, we replaced N_2 with CO_2, thereby increasing the Reynolds number at constant strain rate through a change in the kinematic viscosity of the inert and stretching the Reynolds-dependent entry length. In this way, the flatness of the stagnation surface was considerably improved. Consequently, in the latest set of experiments, such as those discussed in the previous section, CO_2 was used as inert. This first, useful experience is indicative of at least the indirect, and often unexpected, benefits of operating in the unusual microgravity environment. Further studies in microgravity on counterflow flames have been deferred until a new burner that would operate at larger liquid flow rates using an ultrasonic nebulizer is fully tested. The design of a different liquid dispersion system stems from the need to maintain close analogy between experiments and modeling capability. The numerical modeling, currently in progress, requires, in fact, small slip between droplets and gas to preserve self-similarity and one-dimensionality.

Laminar Coflow Diffusion Flames—Normal Gravity
In the experiments on counterflow flames, we saw little or no evidence of individual droplet burning. It is not clear if this observation is indicative of droplet-droplet interactions, that results in droplets evaporating in a cloud at the periphery of which burning occurs, a situation that is typical of practical sprays (ref. 10,11). It could be also an artifact of the particular combination of feed streams, with inert coflow on the fuel side. W decided to examine another configuration, a co-flow axis-symmetric diffusion flame, with the intent to operate at droplet concentrations larger than in the counterflow flames. Analytical models for a Burke-Schumann diffusion flame with fuel spray injection was recently formulated in a configuration that is similar to the one used here (ref. 12). Experimentally, no studies on strictly laminar spray diffusion flames were reported, probably because buoyancy-induced instabilities prevent the establishment of a stable laminar flame at normal gravity, at least under conditions in which there is small slip between the phases (ref. 13). We show below that using the electrospray stable laminar flames can be stabilized in well-controlled combustion environments.

A schematic of the burner is shown in Fig. 1. The typical system to produce a monodisperse electrostatic spray is seen to comprise the metal capillary, through which the liquid fuel is fed, charged at high potential and the porous plate at the top of the burner, that acted as ground electrode. This plate had a 1.9 mm central opening and was positioned at a distance of

0.9 mm downstream of the tip of the capillary where the ES was anchored. Once the cone-jet mode was established, the jet broke up near the plate opening by varicose wave instabilities into a stream of charged droplets. The droplets passed through the opening in the porous plate because their large inertia by far exceeded any electrostatic attraction with the plate. About one millimeter above the plate the stream opened up into a conical fan and ultimately dispersed downstream because of the droplet mutual repulsion. The spray fed a self-sustained, stable, continuous, axis-symmetric, candle-like flame. In the present experiments a co-flow of air at 2.5 l/min was supplied through the burner housing with a uniform velocity of about 5 cm/s. This shroud flow improved the flame stability and ensured overventilated conditions. A small teflon tube, with an inner diameter measuring 4 mm, was mounted coaxially with the capillary, to maintain fuel and oxidizer separated all the way to the burner mouth, and, also, to insulate electrically the capillary from the burner housing. The metal capillary and the teflon tube were kept coaxial by a perforated teflon plate. Gas-phase temperature was determined by an uncoated Pt-6%Rh/Pt-30%Rh thermocouple, whose bead diameter measured 75 μm.

The typical flame had in all respects an appearance very similar to that of a classic candle flame, except that a point source of droplets replaced the candle wick as a source of fuel vapor. Five regions could be readily identified by visual inspection: a) a sharp, bright, blue flame ring, at the very base of the combustion region and perpendicular to the flame axis, that acted as stabilization region of the combustion process; b) a relatively "dark" inner region, that coincided with the bulk of the droplet vaporization region, in the lower part of the flame, right above the flame ring; c) a bright yellow outer "shell" whose luminosity was due to black-body radiation from the soot at high temperature; d) a diffuse, deep blue region in the lower part of the flame, which appeared to envelope the combustion region as the outermost luminous surface; and e) an orange region, at the very top of the flame, that was presumably the soot oxidation region and appeared to be at a lower temperature as compared to the sooty region upstream. Table 1 gives values of relevant parameters for six flames, each numbered in the first column in the table. The key operating variables in each flame are given in the second and third columns in the table. They are the liquid fuel flow rate, Q, and the voltage differential, HV, applied between needle and ground electrode. Changes in these parameters affect the initial size, D_0, and velocity, V_0, of the droplet, that are listed in the fourth and fifth columns, respectively. As a result of variations in the liquid flow rate and applied voltage, the initial droplet size was varied by a factor of two and the initial velocity by about 20%. The height of the ring flame, H_a, of the dark region, H_v, and of the luminous flame, H_t, all measured from the burner plate, are reported in the last three columns of the table.

Figure 2 shows the mean droplet size and velocity measured along the flame centerline for flames, #3, 4 and 5 by the PDA and plotted versus the axial distance from the porous plate. The droplets are "injected" in the combustion region with mean diameters ranging from 52 μm to 58 μm and an initial velocity ranging from 4.33 m/s to 5.0 m/s. In all flames the average droplet size slightly increased in the first few millimeters above the plate, because of the transient heat-up of the droplets and associated decrease in liquid density. Farther downstream the droplet diameters decreased because of evaporation. The Relative Standard Deviation (RSD), that is the ratio of droplet standard deviation to mean diameter, was 0.07 at the first measurement locations, that is the droplets were virtually monodisperse locally. They maintained a very narrow distribution up to z=12 mm. At z= 16 mm the RSD was 0.25. Beyond that point, the size distribution continued to broaden until no droplet signal was detected. At these locations, approximately corresponding to the height of the "dark" zone of each flame (see H_v column in Table 1), evaporation was completed. The data in Fig. 2 show that in their journey along the flame axis the droplets continued to decelerate under the action of the drag force and of the small electric field due to the Coulombic repulsion from the other droplets, the velocity decreasing linearly with axial distance for all flames.

Velocity measurements enable us to convert the spatial abscissa in Fig. 2 into a temporal one and to re-plot the results in Fig. 3 as the square of the diameter versus time, the latter computed from the first measurement location. The goal is to examine whether there are regions of quasi-steady evaporation at least through part of the droplet history. The data show that after an initial transient, the droplets follow the D-square law through a significant portion of their lifetimes in all flames, under conditions in which their size distributions are either monodisperse, or sufficiently narrow to justify the use of mean diameters. The continuous lines in the figure are linear least square fits yielding average evaporation coefficients (mm²/s) of 0.53, 0.57 and 0.60 for Flames #3, 4 and 5, respectively. Remarkably, height measurements and the knowledge of liquid flow rate can *directly* provide average evaporation coefficients of droplets in these spray flames in good agreement with these measurements, as shown in ref. 14. Computation of the evaporation coefficients with the assumption of quasisteady evaporation of an isolated droplet in a convective environment and using the thermocouple measurements on the flame centerline yielded values ranging from 0.72 to 0.80 for Flame #3, from 0.74 to 0.81 for Flame #4 and from 0.78 to 0.84 for Flame #5, all in units of mm²/s. Several factors and uncertainties may have contributed to the discrepancy between the two sets of data, as discussed in Ref. 15. However, the evidence of the applicability of the D-square law in these flames is convincing.

Little or no evidence of individual droplet burning was found in the present experiments. Figure 4 shows the radial scans of temperature at four axial locations under conditions close to those of flame #4. The two lower scans show a pattern with the peak temperature region, that is indicative of the flame location, forming a torus centered on the flame axis, as is typical also of gaseous flames (ref. 16). Farther up into the flame, the trends are the same, albeit the measurements are incomplete because of soot deposition on the thermocouple bead. Eventually, as the flame closed in on the centerline, the location of the temperature peak reached the axis, and the profile would show a monotonically decreasing temperature as a function of radial coordinate. Under individual droplet burning we would expect a much more uniform temperature profile, especially in

the radial direction, in contrast with the data in Fig. 4. Also, since the droplets followed diverging trajectories, we should have been able to discern flame streaks under these conditions. No observations of this sort were made. We conclude that no evidence of individual droplet burning was offered by the present experiments. Rather, conditions were more akin to what is often labeled sheath combustion, with a continuous flame enveloping the entire droplet region and a relatively cooler core in which droplets are evaporating but not burning. Some oxygen was inevitably entrained on the spray axis, since the flames were stabilized approximately three millimeters above the burner plate (see Fig. 6 and the Ha column in Table 1). Yet, stoichiometric conditions in the flame core must have been sufficiently rich to prevent individual droplet burning. In conclusion, even in these relatively dilute sprays, droplet-droplet interactions do prevent individual droplet burning but they do not seem to be sufficient to cause a departure from the D-square law in the flame core.

Since the discussion of group combustion is often cast in terms of the ratio of interdroplet spacing to droplet diameter, l/D, we plotted in Fig. 5 this ratio as a function of radial coordinate at selected axial locations of flame #4, as computed from the inverse cubic root of the measured droplet number density and the size. The vertical bars on each curve of l/D indicate where the peak temperature is at each axial displacement. Also plotted in Fig. 4 is the droplet diameter variation along the radial direction at $z=11.99$ mm, with the length of the vertical bars being equal to two standard deviations of the diameter at every location. In view of the narrowness of the droplet distributions l/D is a meaningful quantity in the present experiments This ratio typically increases along the radial direction, which is a consequence of both the expanding nature of the spray, caused by the droplet coulombic repulsion, and the stronger evaporation at locations closer to the flame, which lead to a monotonic decrease of the number density as function of distance from the spray center. Values of l/D range from 20 on the centerline to about 160 at the outermost location within the spray core enveloped by the flame. Most of the measured values, especially those in the upper portion of the evaporation region, are significantly larger than the typical value of 10-25, that experiments on droplet streams and theoretical models of multiple droplet combustion reported as upper limit for the droplets to start experiencing significant interactions (e.g., ref. 17). This discrepancy is perhaps suggestive of the inadequacy of systems of a small number of droplets, or of a single droplet stream or of even two-dimensional droplet streams to represent properly three-dimensional group combustion that should be relevant to practical spray diffusion combustion system.

The gaseous velocity field on the axis of Flame #4 was also measured using Al_2O_3 particles as tracers for LDV. During the data acquisition, both the droplet velocity and the particle velocity were simultaneously recorded. A typical velocity histogram showed two very distinguishable peaks, one corresponding to the droplet velocity and the other contingent on the presence of the tracers. The average velocity of the particles were then sorted out and the results are plotted in Fig. 6 together with the velocity of droplets as functions of the distance from the burner. Notice that since the sedimentation velocity of micron-size particles is negligible compared with the gas velocity, that was on the order of 1 m/s, the velocity of the particle measured here represents realistically the gas velocity. The gas velocity on the axis of the flame had a complex behavior. It first increase as a result of the transfer of momentum from the droplets that had been injected at velocities two orders of magnitudes larger than the shroud flow. It reached a relative peak in the neighborhood of the anchoring flame, at which point it went through an oscillating behavior , that can be attributed to the expansion from the heat release due to the presence of the ring flame. Farther downstream, after reaching a maximum, it monotonically decreased towards an asymptote at about 1.5 m/s. This behavior differs dramatically from that of gaseous laminar diffusion flames, that are known to be buoyancy controlled (ref. 18). In the latter cases, the velocity on the centerline was shown to be proportional to the square root of the axial displacement. We conclude that the velocity field in this spray flame is in the lower part of the flame momentum-controlled rather than buoyancy-controlled, which may explain why a steady flame could be stabilized in the present situation, unlike the experiments in (ref. 13). Farther downstream, near the flame tip, the low frequency flickering suggests that buoyancy effects becomes significant by inducing local instabilities.

Laminar Coflow Diffusion Flames—Experiments in the 2.2s Drop Tower at NASA Lewis
In the past few weeks we retrofitted the co-flow laminar spray burner to a drop module and observed the spray flame at different flow rates in the 2.2 s tower at NASA Lewis. Two interesting observations were made in these experiments: first, the flame geometry changes dramatically under microgravity conditions, the flame becoming longer, wider and much brighter. This result is in agreement with what was observed in gaseous diffusion flames (ref. 19). It is perhaps surprising the extent of the changes, particularly so in view of the gas-phase velocity measurements on the flame centerline (Fig. 4) that indicated a momentum-controlled flame, at least in the lower part. Second, some of the tallest flames, corresponding to the largest flow rates(#4, 5 and 6), developed instabilities with low frequency (<6 Hz) aperiodic pulsations and relatively large amplitudes. Notice that this behavior is in sharp contrast with that of gaseous diffusion flames. Numerical studies (ref. 20) have shown that the low frequency flickering that is typical of gaseous laminar flames is caused by buoyancy-induced instabilities, which should disappear under microgravity, as confirmed in experiments in ref. 20. On the contrary, for spray flames we found that the instabilities are amplified under certain conditions and affect the entire flame. Future experiments will require longer microgravity times to investigate this phenomenon fully. The numerical modelling of this two-dimensional problem, that is currently under way, will also help understanding this phenomenon. Further details on both the fundamentals of the electrospray and its application to combustion are given in the two Ph. D. dissertations that have resulted from this research (refs. 21 and 22).

Current/Future Plans

Current/future plans include the following tasks: 1) Additional microgravity experiments on the co-flow electrospray diffusion flames have to be performed to allow for longer observation times; 2) We designed, constructed and tested a counterflow spray diffusion flame burner using an ultrasonic nebulizer as spray generator. This system will allow us to operate at larger droplet concentrations and under conditions of small slip between droplets and gas, as dictated by numerical modeling constraints. Once comparisons between experiments and modeling can be performed, we plan to retrofit this apparatus to the Drop Tower and perform experiments in microgravity; 3) We designed and constructed a turbulent spray sytem using an ultrasonic nebulizer, with the intent of systematically studying the effect of turbulent intensity and scale on flame structure. In addition to the capability of measuring droplet size and velocity, we are developing a temperature measurement technique using Raman thermometry; 4) Computational modelling of laminar spray diffusion flames is being pursued under the supervision of Prof. Smooke. Specifically, the droplet phase has been incorporated in existing codes for gaseous flames with detailed tranport and kinetics using a sectional approach. Preliminary results indicate successful convergence for methanol flames and difficulties with the kinetic model for heptane combustion. We plan to revise the heptane kinetic mechanism in the near future. We will also tailor the numerical computation to the experiments in task 2. Finally, we will model two-dimensional co-flow axisymmetric spray diffusion flames to be compared with the experimental counterpart.

References

1. Gomez, A. and Tang, K., "Atomization and Dispersion of Quasi-monodisperse Electrostatic Sprays of Heptane," Proceedings Of the Fifth International Conference on Liquid Atomization and Spray Systems, ICLASS-91, H. G. Semerjian, Ed., NIST Special Publication 813, Gaithersburg, MD, (1991).
2. Gomez, A. and Tang, K., "Characterization of a High Charge Density Electrospray of Methanol", ibid.
3. Gomez, A. and Tang, K., Phys. Fluids A 6, p. 404 (1994).
4. Tang, K. and Gomez, A. Phys. Fluids A 6, p. 2317 (1994).
5. Gomez, A. "The Electrospray: Fundamentals and Applications," Experimental Heat Transfer, Fluid Mechanics and Thermodynamics, Kelleher, M. D. et al., Eds., Vol. 1, p. 270, Elsevier (1993).
6. Chen, G. Gomez, A., Proc. 24th Int. Symposium on Combustion, The Combustion Institute, p. 1531 (1992).
7. Gomez, A.,"The Electrospray: Fundamentals and Combustion Applications," Proceedings of the Second International Microgravity Combustion Workshop, Cleveland (1992).
8. Chen, G. and Gomez, A. "The Individual Effect of Droplet Size and Velocity on the Structure of Counterflow Spray Diffusion Flames," Eastern States Section of the Combustion Institute, Fall Technical Meeting. (1993)
9. Gomez, A. and Chen, G., Combust. Sci. & Tech., 96, p. 47 (1994).
10. Chigier, N. A., Combust. and Flame, 51, p. 127 (1983).
11. Chigier, N.A. and Mc Creath, C.G., Acta Astronautica, 1,p. 687 (1974).
12. Greenberg, J.B.,Combust. Sci. and Tech., 75, p.11 (1991).
13. Levy, Y. and Bulzan, D. "On the Combustion of a Laminar Spray," NASA TM106210, (1993).
14. Gomez, A. and Chen, G. "Experimental Investigation on Self-sustained Co-flow Laminar Diffusion Flames of Monodisperse Sprays," Proceedings of the Sixth International Conference on Liquid Atomization and Spray Systems, ICLASS-94, (A. J. Yule and C. Dumouchel, eds.) p. 718 , Begell House, (1994).
15. Gomez, A. and Chen, G. "Monodisperse Electrosprays: Combustion, Scale-up and Implications for Pollutant Formation", to appear in a volume in the Combustion Science and Technology Book Series (1995).
16. Santoro, R.J., Yeh, T.T., and Semerjian, H.G. , Comb. Sci. & Tech., 53, p.89 (1983) .
17. Sangiovanni; J.J. and M. Labowsky, Combust. and Flame, 47, p. 15 (1982).
18. Gomez, A. and Glassman, I. Proc. 21st Int. Symposium on Combustion, The Combustion Institute, p.1087 (1987).
19. Ellzey, J.L., K.J. Laskey, and E.S. Oran, Comb. and Flame, 84, p. 249 (1991).
20. Bahadori, M.Y. et al. "Effects of Buoyancy on Laminar, Transitional and Turbulent Diffusion Flames," Proceedings of the Second International Microgravity Combustion Workshop, Cleveland (1992).
21. Tang, K. "The Electrospray: Fundamentals and Applications to Targeted Drug Delivery," Ph. D. Thesis, Yale University, 1994.
22. Chen, G. "An Experimental Investigation on Laminar Diffusion Flames of Monodisperse Fuel Sprays, Ph. D. Thesis, Yale University, 1995.

Table 1: Experimental Conditions for the Coflow Diffusion Flames

Flame #	$\dot{Q}$ (ml/hr)	HV (V)	$D_0 (\mu m)$	V_0 (m/s)	H_a (mm)	H_v (mm)	H_t (mm)
1	4.1	1333	34	5.39	3.1	14.1	18.6
2	6.3	1333	46	4.63	3.4	19.7	26.2
3	7.2	1333	52	4.33	2.9	22.6	32.3
4	8.4	1492	52	5.03	3.45	22.6	34.5
5	9.9	1488	58	4.69	3.5	24.6	40.4
6	11.8	1488	67	4.35	3.7	25.8	48.9
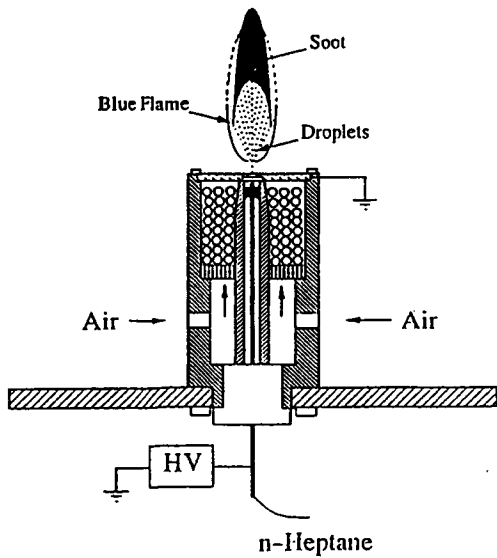
Figure 1.—Schematic of the laminar co-flow spray burner

Figure 2.—Average droplet diameter (D_{10}) (full symbols) and velocity (open symbols) along the centerline of Flame #3 (squares), #4 (triangles) and #5 (circles).
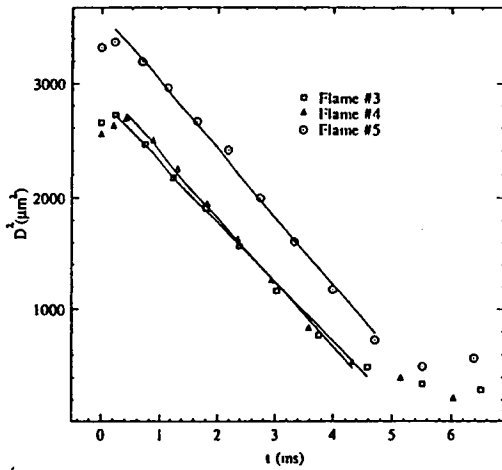

Figure 3.—Square of the average droplet diameter along center line of Flames #3, 4 and 5 vs time. Symbols as in Fig. 2.

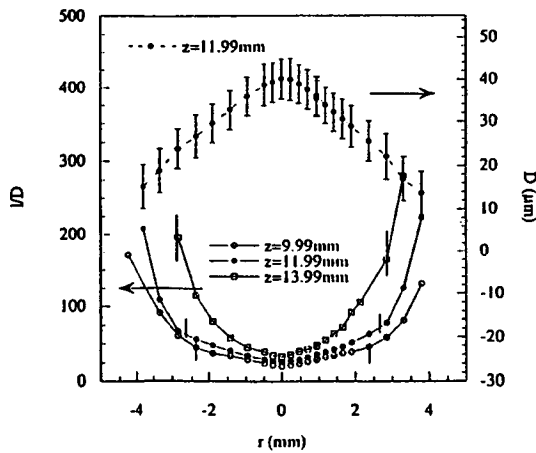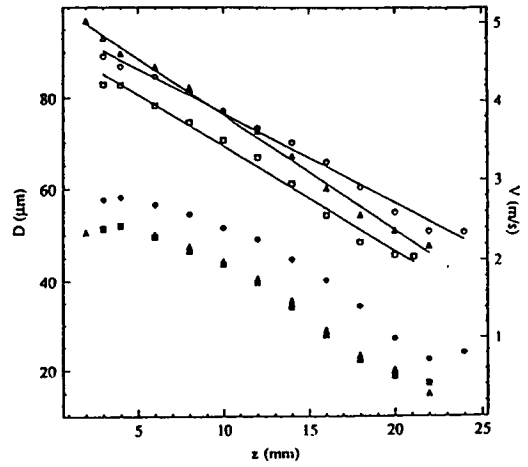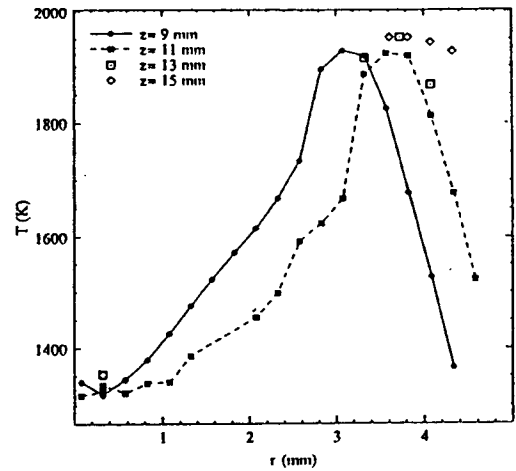Figure 4.—Temperature vs radial coordinate at selected axial locations.

Figure 5.—Radial scan of the ratio of interdroplet spacing over droplet average diameter (left ordinate) and average droplet diameter (right ordinate) at selected axial locations.
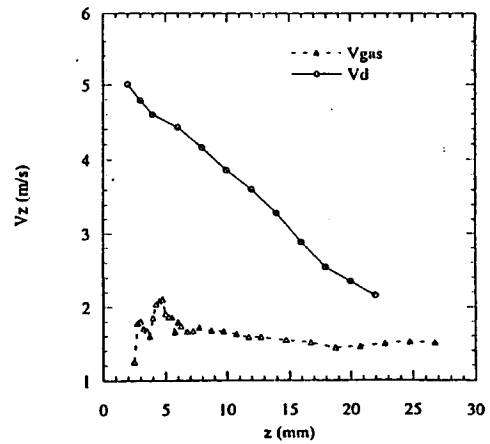

Figure 6.—Average droplet velocity and average gas velocity along the burner axis versus distance from the burner.